J. Fluid Mech. (2023), *vol*. 963, R1, doi:10.1017/jfm.2023.236

New exact Betchov-like relation for the helicity flux in homogeneous turbulence

Damiano Capocci[1],†, Perry L. Johnson[2], Sean Oughton[3], Luca Biferale[1] and Moritz Linkmann[4],†

[1]Department of Physics and INFN, University of Rome Tor Vergata, Rome, Italy

[2]Department of Mechanical and Aerospace Engineering, University of California, Irvine, CA 92697-2700, USA

[3]Department of Mathematics, University of Waikato, Hamilton, New Zealand

[4]School of Mathematics and Maxwell Institute for Mathematical Sciences, University of Edinburgh, Edinburgh EH9 3FD, UK

(Received 10 January 2023; revised 10 March 2023; accepted 11 March 2023)

In homogeneous and isotropic turbulence, the relative contributions of different physical mechanisms to the energy cascade can be quantified by an exact decomposition of the energy flux (Johnson, *Phys. Rev. Lett.*, vol. 124, 2020, 104501; *J. Fluid Mech.*, vol. 922, 2021, A3). We extend the formalism to the transfer of kinetic helicity across scales, important in the presence of large-scale mirror-breaking mechanisms, to identify physical processes resulting in helicity transfer and quantify their contributions to the mean flux in the inertial range. All subfluxes transfer helicity from large to small scales. Approximately 50 % of the mean flux is due to the scale-local vortex flattening and vortex twisting. We derive a new exact relation between these effects, similar to the Betchov relation for the energy flux, revealing that the mean contribution of the former is three times larger than that of the latter. Multi-scale effects account for the remaining 50 % of the mean flux, with approximate equipartition between multi-scale vortex flattening, twisting and entangling.

Key words: homogeneous turbulence, turbulence theory

1. Introduction

The kinetic helicity, defined as the L^2-inner product of velocity $\boldsymbol{u}$ and vorticity $\boldsymbol{\omega}$, has dynamical, topological, geometrical and statistical interpretations in turbulence. It is a dynamical and topological inviscid invariant, where the latter refers to its connection with the linking number of infinitesimal vortex lines (Moffatt 1969). Geometrically, it quantifies the alignment of velocity and vorticity in a volume-averaged sense. Within a

† Email addresses for correspondence: capocci@roma2.infn.it, moritz.linkmann@ed.ac.uk

statistical approach to turbulence, helicity is the correlation between velocity and vorticity. In a rotationally invariant ensemble, it is connected to the breaking of the symmetry under inversion of all axes. Inspired by its relevance to turbulence in atmospheric flows (Lilly 1986), dynamical and statistical effects connected with helicity have been studied in the atmospheric boundary layer (Deusebio & Lindborg 2014) and in rotating turbulence (Mininni & Pouquet 2010*a*,*b*), and more generally in homogeneous and isotropic turbulence (Chen, Chen & Eyink 2003*a*; Chen *et al.* 2003*b*; Gledzer & Chkhetiani 2015; Kessar *et al.* 2015; Sahoo, Bonaccorso & Biferale 2015; Stepanov *et al.* 2015; Alexakis 2017; Sahoo, Alexakis & Biferale 2017; Yan *et al.* 2020; Milanese, Loureiro & Boldyrev 2021), as well as shear flows (Yan *et al.* 2020; Yu *et al.* 2022) and in laboratory experiments (Scheeler *et al.* 2017).

The level of helicity in a turbulent flow affects turbulent statistics and dynamics, and is thus of relevance from a fundamental theory perspective as well as for subgrid-scale (SGS) modelling. As an alignment of velocity and vorticity weakens the nonlinearity of the Navier–Stokes equations, high levels of helicity have been connected with a depletion of the kinetic energy flux across scales by an analysis of the coupling between helical Fourier modes (Kraichnan 1973), and with regions of low dissipation (Moffatt 2014). These effects can be quantified by upper bound theory applied to helical forcing and direct numerical simulation – the energy flux of turbulence sustained by fully helical forcing is approximately 30 % lower than in the non-helical case (Linkmann 2018).

Helicity affects turbulence not only globally, that is, in terms of mean energy fluxes, but also on a scale-by-scale level. As a solenoidal vector field, the velocity field $\boldsymbol{u}$ can be decomposed into positively and negatively helical components $\boldsymbol{u}^{\pm}$ (Herring 1974; Constantin & Majda 1988; Waleffe 1992), $\boldsymbol{u}(\boldsymbol{x}, t) = \boldsymbol{u}^{+}(\boldsymbol{x}, t) + \boldsymbol{u}^{-}(\boldsymbol{x}, t)$, where $\boldsymbol{u}^{\pm}$ are obtained by projecting the Fourier coefficients $\hat{\boldsymbol{u}}(\boldsymbol{k}, t)$ onto basis vectors which are eigenfunctions of the curl operator in Fourier space. That is, $\hat{\boldsymbol{u}}^{\pm}(\boldsymbol{k}, t) = u^{\pm}(\boldsymbol{k}, t)\boldsymbol{h}^{\pm}(\boldsymbol{k})$, where $i\boldsymbol{k} \times k\boldsymbol{h}^{\pm}(\boldsymbol{k}) = \pm\boldsymbol{h}^{\pm}(\boldsymbol{k})$ and $u^{\pm}(\boldsymbol{k}, t) = \hat{\boldsymbol{u}}(\boldsymbol{k}, t)\cdot\boldsymbol{h}^{\pm}(\boldsymbol{k})$. The energy flux can then be decomposed into different triadic couplings between positively and negatively helical velocity-field fluctuations (Waleffe 1992). Interestingly, interactions among helical Fourier modes of like-signed helicity lead to an inverse energy transfer across scales in the inertial range (Waleffe 1992; Biferale, Musacchio & Toschi 2012, 2013; Sahoo *et al.* 2015), while interactions of oppositely-signed helical modes transfer energy from large to small scales (Waleffe 1992; Alexakis 2017; Alexakis & Biferale 2018). For turbulent flows of electrically conducting fluids, such as liquid metals or plasmas in the fluid approximation, helicity alters the evolution of both velocity and magnetic-field fluctuations profoundly. Here, small-scale kinetic helicity facilitates the formation of large-scale coherent magnetic structures through the large-scale dynamo (Steenbeck, Krause & Rädler 1966; Brandenburg 2001; Brandenburg & Subramanian 2005; Tobias, Cattaneo & Boldyrev 2013; Linkmann *et al.* 2016, 2017).

The cascade of kinetic helicity itself is predicted to be direct, that is, it proceeds from large to small scales (Brissaud *et al.* 1973; Waleffe 1992), and scale-local (Eyink 2005). It results, as discussed by Eyink (2006) in the context of a multi-scale gradient expansion, from a twisting of small-scale vortices into a local alignment with the small-scale velocity fluctuations by large-scale differential vorticity ('screw'). However, being sign-indefinite, numerical results on helicity fluxes can be difficult to interpret as a loss of positive helicity at a given scale may be viewed as a gain of negative helicity at the same scale.

In the context of SGS modelling, the effect helicity has on a turbulent flow is usually taken into account through additional diffusive model terms (Yokoi & Yoshizawa 1993; Li *et al.* 2006; Baerenzung *et al.* 2008; Inagaki, Yokoi & Hamba 2017). However, a combination of *a priori* and *a posteriori* analyses of different SGS models for isotropic

helical turbulence found the effect of the additional diffusive model terms to be small and that a classical Smagorinsky model best represents the resolved-scale dynamics (Li *et al.* 2006). Similarly, based on analytical and numerical results, Linkmann (2018) suggests an adjustment of the Smagorinsky constant to account for high levels of helicity. So far, SGS analyses of helical turbulence have mainly been concerned with energy transfers.

Here, we focus on the helicity flux across scales in statistically stationary homogeneous and isotropic turbulence, with large-scale forcing breaking mirror symmetry. For the energy flux, the Betchov (1956) relation states that the mean contribution from vortex stretching to the energy cascade is triple that due to strain self-amplification. Carbone & Wilczek (2022) recently showed that there are no further kinematic relations for the energy flux in statistically stationary homogeneous and isotropic turbulence with zero net helicity. However, we prove here that a new exact kinematic Betchov-type relation exists for the mean helicity flux. Furthermore, we also present an exact decomposition of the helicity flux in analogy to that of the kinetic energy flux derived by Johnson (2020, 2021), whereby the relative contributions of physical mechanisms, such as vortex stretching and strain self-amplification, to the energy cascade can be quantified in terms of the overall contribution and their scale locality. The aim is to identify physical mechanisms that transfer kinetic helicity across scales and to quantify their relative contributions to the mean helicity flux and its fluctuations, which may be useful for the construction of SGS models when resolving the helicity cascade is of interest.

2. Exact decomposition of the kinetic helicity flux

To derive the aforementioned exact decomposition of the helicity flux and relations between the resulting subfluxes, we begin with the three-dimensional (3-D) incompressible Navier–Stokes equations, here written in component form:

$$\partial_t u_i + \partial_j \left(u_i u_j\right) = -\partial_j p \delta_{ij} + 2\nu \partial_j S_{ij} + f_i, \tag{2.1}$$

$$\partial_j u_j = 0, \tag{2.2}$$

where $\boldsymbol{u} = (u_1, u_2, u_3)$ is the velocity field, p the pressure divided by the constant density, ν the kinematic viscosity, S_{ij} the rate-of-strain tensor and $\boldsymbol{f} = (f_1, f_2, f_3)$ an external solenoidal force that may be present. To define the helicity flux across scales, we introduce a filtering operation to separate large- and small-scale dynamics (e.g. Germano 1992). Specifically, for a generic function ϕ, the filtered version at scale ℓ is $\bar{\phi}^\ell = G^\ell * \phi$, where G^ℓ is a filter kernel with filter width ℓ and the asterisk denotes the convolution operation. Applying the filter to the Navier–Stokes equations (2.1)–(2.2) results in

$$\partial_t \bar{u}_i^\ell + \partial_j \left(\bar{u}_i^\ell \bar{u}_j^\ell + \bar{p}^\ell \delta_{ij} - 2\nu \bar{S}_{ij}^\ell + \tau_{ij}^\ell\right) = \bar{f}_i^\ell, \tag{2.3}$$

where $\tau_{ij}^\ell = \tau^\ell(u_i, u_j) = \overline{u_i u_j}^\ell - \bar{u}_i^\ell \bar{u}_j^\ell$ is the SGS stress tensor. Here, we follow the notation of Germano (1992) in defining the generalised second moment for any two fields as $\tau^\ell(a, b) = \overline{ab}^\ell - \bar{a}^\ell \bar{b}^\ell$. We also require the filtered vorticity equation

$$\partial_t \bar{\omega}_i^\ell + \partial_j \left(\bar{\omega}_i^\ell \bar{u}_j^\ell - \bar{u}_i^\ell \bar{\omega}_j^\ell - \nu \partial_j \bar{\omega}_i^\ell\right) - \bar{g}_i^\ell = -\partial_j \left(\epsilon_{imn} \partial_m \tau_{nj}^\ell\right), \tag{2.4}$$

where $\boldsymbol{g} = \boldsymbol{\nabla} \times \boldsymbol{f}$. The large-scale helicity density, $H^\ell = \bar{u}_i^\ell \bar{\omega}_i^\ell$, then evolves according to

$$\begin{aligned} \partial_t H^\ell + \partial_j \left[H^\ell \bar{u}_j^\ell + (\bar{p}^\ell - \tfrac{1}{2}\bar{u}_i^\ell \bar{u}_i^\ell)\bar{\omega}_j^\ell - \nu \partial_j H^\ell\right] + 2\nu(\partial_j \bar{u}_i^\ell)(\partial_j \bar{\omega}_i^\ell) - \bar{\omega}_i^\ell \bar{f}_i^\ell - \bar{u}_i^\ell \bar{g}_i^\ell \\ = -\partial_j \left[2\bar{\omega}_i^\ell \tau_{ij}^\ell + \epsilon_{ijk} \bar{u}_i^\ell \partial_m \tau_{km}^\ell\right] + 2\tau_{ij}^\ell \partial_j \bar{\omega}_i^\ell. \end{aligned} \tag{2.5}$$

The last term in this equation is the helicity flux

$$\Pi^{H,\ell} = -2\tau_{ij}^{\ell}\partial_j\bar{\omega}_i^{\ell}, \tag{2.6}$$

and is the central focus herein. It has an alternative form (Yan *et al.* 2020),

$$\tilde{\Pi}^{H,\ell} = -\tau_{ij}^{\ell}\partial_j\bar{\omega}_i^{\ell} - \left[\tau^{\ell}(\omega_i, u_j) - \tau^{\ell}(u_i, \omega_j)\right]\partial_j\bar{u}_i^{\ell}, \tag{2.7}$$

and it can be shown that the right-hand side of (2.6) and (2.7) differ by an expression that can be written as a divergence and therefore vanishes after averaging spatially, at least for statistically homogeneous turbulence (Yan *et al.* 2020). This implies $\langle\Pi^{H,\ell}\rangle = \langle\tilde{\Pi}^{H,\ell}\rangle$. Eyink (2006) links the first term in (2.7) – which is proportional to $\Pi^{H,\ell}$ – to vortex twisting and Yan *et al.* (2020) attribute the second term to vortex stretching. In what follows we discuss an exact decomposition of $\Pi^{H,\ell}$, and show that both effects can be identified therein. We also use $\Pi^{H,\ell}$ for our numerical evaluations (cf. Chen *et al.* 2003*a*; Eyink 2006).

2.1. *Gaussian filter relations for the helicity flux*

So far all expressions are exact and filter-independent. To derive exact decompositions of the helicity flux in both representations, we now focus on Gaussian filters. For that case, Johnson (2020, 2021) showed that the SGS stresses can be obtained as the solution of a forced diffusion equation with ℓ^2 being the time-like variable, resulting in

$$\tau_{ij}^{\ell} = \tau^{\ell}(u_i, u_j) = \ell^2\bar{A}_{ik}^{\ell}\bar{A}_{jk}^{\ell} + \int_0^{\ell^2} \mathrm{d}\theta\ \tau^{\phi}\left(\bar{A}_{ik}^{\sqrt{\theta}}, \bar{A}_{kj}^{\sqrt{\theta}}\right), \tag{2.8}$$

where $\phi(\theta) = \sqrt{\ell^2 - \theta}$ and $A_{ij} = \partial_j u_i$ are the velocity-field gradients. Since the SGS stress tensor τ_{ij}^{ℓ} is symmetric, for the first form of the helicity flux we obtain in analogy to the energy flux

$$\Pi^{H,\ell} = -2\tau_{ij}^{\ell}\bar{S}_{\omega,ij}^{\ell}, \tag{2.9}$$

where S_ω is the symmetric component of the vorticity gradient tensor, with components $S_{\omega,ij} = (\partial_j\omega_i + \partial_i\omega_j)/2$. Employing (2.8) this yields

$$\Pi^{H,\ell} = -2\ell^2\bar{S}_{\omega,ij}^{\ell}\bar{A}_{ik}^{\ell}\bar{A}_{jk}^{\ell} - 2\int_0^{\ell^2} \mathrm{d}\theta\ \bar{S}_{\omega,ij}^{\ell}\tau^{\phi}\left(\bar{A}_{ik}^{\sqrt{\theta}}, \bar{A}_{kj}^{\sqrt{\theta}}\right). \tag{2.10}$$

The first term involves a product of gradient tensors filtered at the same scale, ℓ; hence we refer to it as being single-scale, and denote it $\Pi_s^{H,\ell}$. In mean, it coincides with the nonlinear LES model for the SGS stresses (Eyink 2006). In contrast, the second term encodes the correlation between resolved-scale vorticity-field gradients and (summed) velocity-field gradients at each scale smaller than ℓ, so that we refer to it as multi-scale.

Splitting the velocity gradient tensors into symmetric and antisymmetric parts, that is, into the rate-of-strain tensor $\boldsymbol{S} = (\boldsymbol{A} + \boldsymbol{A}^t)/2$ and vorticity tensor $\boldsymbol{\Omega} = (\boldsymbol{A} - \boldsymbol{A}^t)/2$, where

$\boldsymbol{A}^t$ is the transpose of $\boldsymbol{A}$, the helicity flux can be decomposed into six subfluxes:

$$\Pi^{H,\ell} = \Pi^{H,\ell}_{s,SS} + \Pi^{H,\ell}_{s,\Omega\Omega} + \Pi^{H,\ell}_{s,S\Omega} + \Pi^{H,\ell}_{m,SS} + \Pi^{H,\ell}_{m,\Omega\Omega} + \Pi^{H,\ell}_{m,S\Omega}, \tag{2.11}$$

where the single-scale terms are

$$\Pi^{H,\ell}_{s,SS} = -2\ell^2 \bar{S}^\ell_{\omega,ij}\bar{S}^\ell_{ik}\bar{S}^\ell_{jk} = -2\ell^2 \mathrm{tr}\left\{(\bar{\boldsymbol{S}}^\ell_\omega)^t \bar{\boldsymbol{S}}^\ell (\bar{\boldsymbol{S}}^\ell)^t\right\}, \tag{2.12}$$

$$\Pi^{H,\ell}_{s,\Omega\Omega} = -2\ell^2 \bar{S}^\ell_{\omega,ij}\bar{\Omega}^\ell_{ik}\bar{\Omega}^\ell_{jk} = -2\ell^2 \mathrm{tr}\left\{(\bar{\boldsymbol{S}}^\ell_\omega)^t \bar{\boldsymbol{\Omega}}^\ell (\bar{\boldsymbol{\Omega}}^\ell)^t\right\}, \tag{2.13}$$

$$\Pi^{H,\ell}_{s,S\Omega} = -2\ell^2 \bar{S}^\ell_{\omega,ij}\left(\bar{S}^\ell_{ik}\bar{\Omega}^\ell_{jk} - \bar{\Omega}^\ell_{ik}\bar{S}^\ell_{jk}\right) = -4\ell^2 \mathrm{tr}\left\{(\bar{\boldsymbol{S}}^\ell_\omega)^t \bar{\boldsymbol{S}}^\ell (\bar{\boldsymbol{\Omega}}^\ell)^t\right\}, \tag{2.14}$$

and tr $\{\cdot\}$ denotes the trace. We purposefully retained the transposition operation here also for symmetric tensors to show what the approach needs to be when the tensors involved are not symmetric. Similarly, the multi-scale terms are

$$\Pi^{H,\ell}_{m,SS} = -2\int_0^{\ell^2} \mathrm{d}\theta\ \bar{S}^\ell_{\omega,ij}\tau^\phi\left(\bar{S}^{\sqrt{\theta}}_{ik}, \bar{S}^{\sqrt{\theta}}_{kj}\right), \tag{2.15}$$

$$\Pi^{H,\ell}_{m,\Omega\Omega} = 2\int_0^{\ell^2} \mathrm{d}\theta\ \bar{S}^\ell_{\omega,ij}\tau^\phi\left(\bar{\Omega}^{\sqrt{\theta}}_{ik}, \bar{\Omega}^{\sqrt{\theta}}_{kj}\right), \tag{2.16}$$

$$\begin{aligned}\Pi^{H,\ell}_{m,S\Omega} &= -2\int_0^{\ell^2} \mathrm{d}\theta\ \bar{S}^\ell_{\omega,ij}\left[\tau^\phi\left(\bar{S}^{\sqrt{\theta}}_{ik}, \bar{\Omega}^{\sqrt{\theta}}_{jk}\right) + \tau^\phi\left(\bar{\Omega}^{\sqrt{\theta}}_{ik}, \bar{S}^{\sqrt{\theta}}_{jk}\right)\right] \\ &= -4\int_0^{\ell^2} \mathrm{d}\theta\ \bar{S}^\ell_{\omega,ij}\tau^\phi\left(\bar{S}^{\sqrt{\theta}}_{ik}, \bar{\Omega}^{\sqrt{\theta}}_{jk}\right).\end{aligned} \tag{2.17}$$

We recall that $\langle \Pi^{H,\ell}_{s,\Omega\Omega}\rangle$, the spatial average of the contribution to the helicity flux due to coupling of resolved-scale vorticity strain with resolved-scale vorticity, vanishes,

$$\langle \Pi^{H,\ell}_{s,\Omega\Omega}\rangle = -\frac{\ell^2}{4}\left\langle\left(\partial_j\bar{\omega}^\ell_i + \partial_i\bar{\omega}^\ell_j\right)\bar{\omega}^\ell_i\bar{\omega}^\ell_j\right\rangle = -\frac{\ell^2}{4}\left\langle\partial_j(\bar{\omega}^\ell_i\bar{\omega}^\ell_i\bar{\omega}^\ell_j)\right\rangle = 0, \tag{2.18}$$

due to periodic boundary conditions and the divergence-free nature of the vorticity field, as previously discussed by Eyink (2006) in the context of a multi-scale gradient expansion of the SGS stress tensor.

The physics encoded in these transfer terms may be understood in terms of three effects: (i) 'vortex flattening' – compression and stretching of a vortex tube into a vortex sheet by large-scale straining motion, with the principal axes of the vorticity deformation tensor S_ω aligning with that of the strain-rate tensor at smaller scale, see (2.12) and (2.15); (ii) 'vortex twisting' – a twisting of small-scale vortex tubes by large-scale differential vorticity into thinner tubes consisting of helical vortex lines, and subsequent small-scale alignment between the resulting vorticity vectors and the extensile stress generated thereby (Eyink 2006), see (2.14) and (2.17); and (iii) 'vortex entangling' – twisting of entangled vortex lines, see (2.13) and (2.16). Interpreting helicity as the correlation between velocity and vorticity, a change in this correlation (or alignment) across scales occurs by vorticity deformation through straining motions or differential vorticity. This results in decorrelation at large scales and an increase in small-scale correlation.

The interpretation of vortex entangling, or twisting of entangled vortex lines, relies on the topological interpretation of helicity in terms of link, twist and writhe of vortex tubes.

The terms we interpret in this way do not involve strain-rate tensors; they only involve vorticity and differential vorticity. As such they describe vortex–vortex interactions driven by a twisting and stretching of a bundle of vortex tubes by differential vorticity. If we consider a single bundle of vortex tubes, writhe is a global (or large-scale) quantity in the sense that one needs to consider the entire bundle to describe it. In contrast, twist is a local (or small-scale) concept that describes the winding of the entangled vortex tubes that constitute the bundle around each other (Scheeler *et al.* 2017). What we loosely describe as 'twisting of entangled vortex lines' can be thought of as a writhe-to-twist transfer of helicity, by deformation of the vortex bundle, see e.g. Scheeler *et al.* (2017). This would necessarily be a multi-scale process, and indeed we see in (2.18) that the single-scale term $\langle \Pi^{H,\ell}_{s,\Omega\Omega}\rangle$ vanishes in mean.

2.2. *An exact Betchov-type relation for the helicity flux*

In homogeneous turbulence, the Betchov (1956) relation is an exact expression connecting the contributions associated with vortex stretching and strain self-amplification to the mean energy flux across scales. Here we show that there is an analogous exact expression relating two (single-scale) mean helicity subfluxes: $3\langle \Pi^{H,\ell}_{s,SS}\rangle = \langle \Pi^{H,\ell}_{s,S\Omega}\rangle$. These subfluxes are associated with vortex flattening, $\langle \Pi^{H,\ell}_{s,SS}\rangle$, and vortex twisting, $\langle \Pi^{H,\ell}_{s,S\Omega}\rangle$. Written in terms of the definitions given in (2.12) and (2.14), this expression reads

$$3\left\langle \mathrm{tr}\left\{\bar{\boldsymbol{S}}^{\ell}_{\omega}\bar{\boldsymbol{S}}^{\ell}\bar{\boldsymbol{S}}^{\ell}\right\}\right\rangle = 2\left\langle \mathrm{tr}\left\{\bar{\boldsymbol{S}}^{\ell}_{\omega}\bar{\boldsymbol{\Omega}}^{\ell}\bar{\boldsymbol{S}}^{\ell}\right\}\right\rangle. \tag{2.19}$$

Before proceeding to a proof of this expression, we point out that it is a relation between the respective traces of two tensors, that is, geometric objects. Consequently, (2.19) is independent of the filter kernel and indeed also holds for the un-filtered case. Here, we embed the derivation within the framework developed in § 2.1 so as to remain focused on the physical interpretation of the terms in (2.19) as subfluxes across scales.

The main steps in a proof of (2.19) are now summarised. Following an argument analogous to that used in proving the Betchov (1956) relation for the energy flux, and using tensor symmetry properties and (2.18), one obtains (Eyink 2006)

$$\left\langle \mathrm{tr}\left\{\bar{\boldsymbol{S}}^{\ell}_{\omega}\bar{\boldsymbol{S}}^{\ell}\bar{\boldsymbol{S}}^{\ell}\right\}\right\rangle = -\left\langle \mathrm{tr}\left\{\bar{\boldsymbol{\Omega}}^{\ell}_{\omega}(\bar{\boldsymbol{S}}^{\ell}\bar{\boldsymbol{\Omega}}^{\ell}+\bar{\boldsymbol{\Omega}}^{\ell}\bar{\boldsymbol{S}}^{\ell})\right\}\right\rangle = -2\left\langle \mathrm{tr}\left\{\bar{\boldsymbol{\Omega}}^{\ell}_{\omega}\bar{\boldsymbol{\Omega}}^{\ell}\bar{\boldsymbol{S}}^{\ell}\right\}\right\rangle, \tag{2.20}$$

where Ω_ω is the antisymmetric part of the vorticity gradient tensor. This yields

$$\frac{1}{2}\left\langle \mathrm{tr}\left\{\nabla\bar{\boldsymbol{\omega}}^{\ell}\left(\nabla\bar{\boldsymbol{u}}^{\ell}\right)^{t}\left[\nabla\bar{\boldsymbol{u}}^{\ell}+\left(\nabla\bar{\boldsymbol{u}}^{\ell}\right)^{t}\right]\right\}\right\rangle = \left\langle \mathrm{tr}\left\{\frac{3}{2}\,\bar{\boldsymbol{S}}^{\ell}_{\omega}\bar{\boldsymbol{S}}^{\ell}\bar{\boldsymbol{S}}^{\ell}-\bar{\boldsymbol{S}}^{\ell}_{\omega}\bar{\boldsymbol{\Omega}}^{\ell}\bar{\boldsymbol{S}}^{\ell}\right\}\right\rangle. \tag{2.21}$$

Thus, showing that the left-hand side of this expression vanishes will prove the Betchov relation for the helicity flux, (2.19). To do so, we express the left-hand side of (2.21) using the chain rule and in index notation

$$\begin{aligned}\left\langle \partial_j\bar{\omega}^{\ell}_i\partial_j\bar{u}^{\ell}_k\bar{S}^{\ell}_{ki}\right\rangle = {}& \left\langle \partial_j\left[\bar{\omega}^{\ell}_i\partial_j\bar{u}^{\ell}_k\bar{S}^{\ell}_{ki}\right]\right\rangle - \left\langle \bar{\omega}^{\ell}_i\partial_j\partial_j\bar{u}^{\ell}_k\bar{S}^{\ell}_{ki}\right\rangle \\ & - \left\langle \bar{\omega}^{\ell}_i\bar{S}^{\ell}_{kj}\partial_j\bar{S}^{\ell}_{ki}\right\rangle - \left\langle \bar{\omega}^{\ell}_i\bar{\Omega}^{\ell}_{kj}\partial_j\bar{S}^{\ell}_{ki}\right\rangle.\end{aligned} \tag{2.22}$$

The first term on the right-hand side of this expression vanishes making use of periodic boundary conditions. Using incompressibility and integration by parts it can be shown that the last term also vanishes. The two remaining terms cancel out, which is shown by similar arguments and using the properties of the Levi-Civita tensor. This completes the proof.

N	E	ν	ε	ε_H	L	τ	Re_λ	$\eta/10^{-3}$	k_{max}	$k_{max}\eta$	$\Delta t/\tau$	No.
1024	7.26	0.001	3.33	5.02	1.12	0.50	327	4.20	340	1.43	0.60	39

Table 1. Simulation parameters and key observables, where N is the number of collocation points in each coordinate, E the (mean) total kinetic energy, ν the kinematic viscosity, ε the mean energy dissipation rate, ε_H the mean helicity dissipation rate, $L = (3\pi/4E)\int_0^{k_{max}} \mathrm{d}k\ E(k)/k$ the integral scale, $\tau = L/\sqrt{2E/3}$ the large-eddy turnover time, Re_λ the Taylor-scale Reynolds number, $\eta = (\nu^3/\varepsilon)^{1/4}$ the Kolmogorov microscale, k_{max} the largest wavenumber after de-aliasing, Δt the sampling interval which is calculated from the length of the averaging interval divided by the number of equispaced snapshots, and 'No.' the number of snapshots. The data corresponds to run 22 of Sahoo *et al.* (2017). It is available for download using the SMART-Turb portal http://smart-turb.roma2.infn.it.

The mean single-scale terms also arise as the first-order contribution in a multi-scale expansion of the SGS stress tensor (Eyink 2006), where (2.20) is used to deduce that the full vorticity gradient, not only either its symmetric or antisymmetric component, is involved in the helicity flux across scales. In consequence, (2.19) and (2.20) assert that the mean transfers involving the symmetric or the antisymmetric parts of the vorticity gradient can be related to one another, and thus the single-scale contribution to the mean helicity flux can be written as

$$\left\langle \Pi_s^{H,\ell} \right\rangle = -8\ell^2 \left\langle \mathrm{tr}\left\{ \bar{\boldsymbol{S}}_\omega^\ell \bar{\boldsymbol{S}}^\ell \bar{\boldsymbol{S}}^\ell \right\} \right\rangle = -\frac{16}{3}\ell^2 \left\langle \mathrm{tr}\left\{ \bar{\boldsymbol{S}}_\omega^\ell \bar{\boldsymbol{\Omega}}^\ell \bar{\boldsymbol{S}}^\ell \right\} \right\rangle. \tag{2.23}$$

3. Numerical details and data

Data has been generated by direct numerical simulation of the incompressible 3-D Navier–Stokes equations (2.1) and (2.2) on a triply periodic domain of size $L_{box} = 2\pi$ in each direction, where the forcing $\boldsymbol{f}$ is a random Gaussian process with zero mean, fully helical $\boldsymbol{f} = \boldsymbol{f}^+$, and active in the wavenumber band $k \in [0.5, 2.4]$. The spatial discretisation is implemented through the standard, fully dealiased pseudospectral method with 1024 collocation points in each direction. Further details and mean values of key observables are summarised in table 1.

Figure 1(*a*) presents the time series of the total kinetic energy per unit volume, $E(t)$. Time-averaged kinetic energy spectra of positively and negatively helical fluctuations, $E^\pm(k) = \langle \frac{1}{2}\sum_{k\le|\boldsymbol{k}|<k+1} |\hat{\boldsymbol{u}}^\pm(\boldsymbol{k})|^2 \rangle$ and the total energy spectrum $E(k) = E^+(k) + E^-(k)$, are shown in Kolmogorov-compensated form in figure 1(*b*). As can be seen by comparison of $E^+(k)$ and $E^-(k)$, the large-scale velocity-field fluctuations are dominantly positively helical, which is a consequence of the forcing. Decreasing in scale, we observe that negatively helical fluctuations increase in amplitude, and approximate equipartition between $E^+(k)$ and $E^-(k)$ is reached for $k\eta \ge 0.2$. That is, a helically forced turbulent flow, where mirror symmetry is broken at and close to the forcing scale, restores mirror symmetry at smaller scales through nonlinear interactions (Chen *et al.* 2003*a*; Deusebio & Lindborg 2014; Kessar *et al.* 2015).

4. Numerical results for mean subfluxes and fluctuations

Figure 2 shows the total helicity flux and all subfluxes, normalised by the total helicity dissipation rate ε_H. As can be seen in the figure, the term $\langle \Pi_{s,\Omega\Omega}^{H,\ell} \rangle$ is identically zero, which must be the case according to (2.18). Moreover, the helicity Betchov relation (2.19)

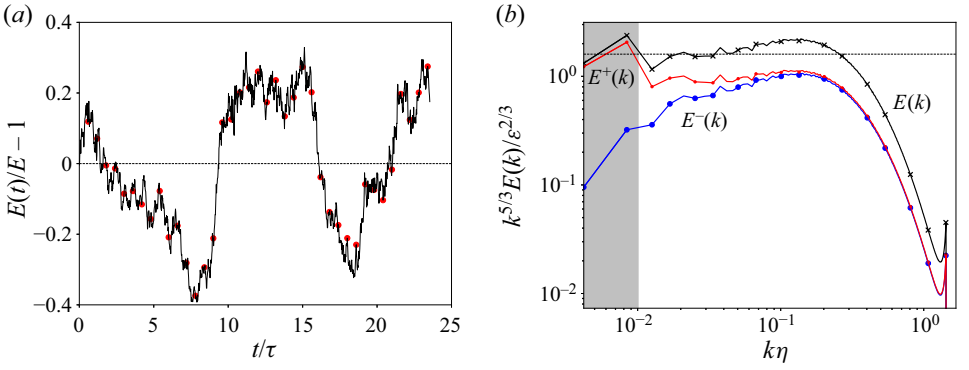

Figure 1. (*a*) Time evolution of the total energy normalised by its mean value, E. Time is given in units of large-eddy turnover time τ. The red dots correspond to the sampled velocity-field configurations. (*b*) Time-averaged energy spectra in Kolmogorov-compensated form. The grey-shaded area indicates the forcing range. The dashed line indicates a Kolmogorov constant $C_K \approx 1.6$.

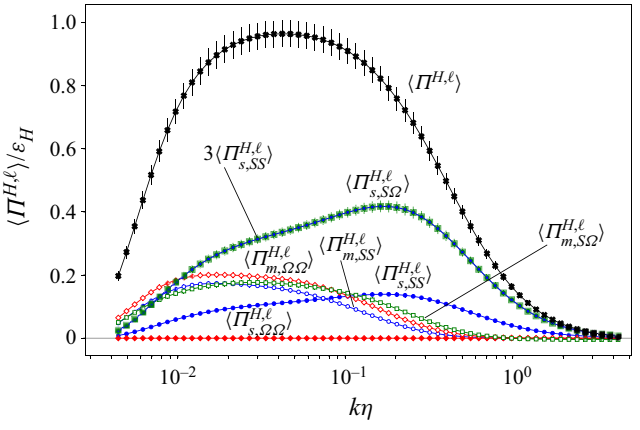

Figure 2. Decomposed helicity fluxes normalised with the mean helicity dissipation rate ε_H. Filled markers correspond to single-scale contributions while empty symbols are related to multi-scale contributions. The error bars indicate one standard error. The subflux $\langle \Pi^{H,\ell}_{s,S\Omega} \rangle$ has been superposed with $3\langle \Pi^{H,\ell}_{s,SS} \rangle$ in order to highlight the Betchov-type relation (2.19).

derived here is satisfied as it must be – the terms $\langle \Pi^{H,\ell}_{s,S\Omega} \rangle$ and $3\,\langle \Pi^{H,\ell}_{s,SS} \rangle$ are visually indistinguishable, with a relative error between them of order 10^{-6} (not shown). A few further observations can be made from the data. The non-vanishing multi-scale terms, $\langle \Pi^{H}_{m,S\Omega} \rangle$, $\langle \Pi^{H}_{m,SS} \rangle$ and $\langle \Pi^{H}_{m,\Omega\Omega} \rangle$ are comparable in magnitude across all scales. They are approximately scale-independent in the interval $10^{-2} \leq k\eta \leq 10^{-1}$, with each accounting for approximately 15–20 % of the total helicity flux in this range of scales. Even though clear plateaux are not present for the two non-vanishing single-scale terms, $\langle \Pi^{H}_{s,S\Omega} \rangle$ and $\langle \Pi^{H}_{s,SS} \rangle$, one could tentatively extrapolate that at higher Re, approximately 30 % of the mean flux originates from scale-local vortex twisting and 10 % from vortex flattening. That is, the multi-scale contributions amount to 50–60 % and the scale-local contributions to 40–50 % of the total helicity flux across scales, at least for this particular simulation.

Having discussed the mean subfluxes, we now consider the fluctuations of each subflux term, in order to quantify the level of fluctuations in each term and the presence and

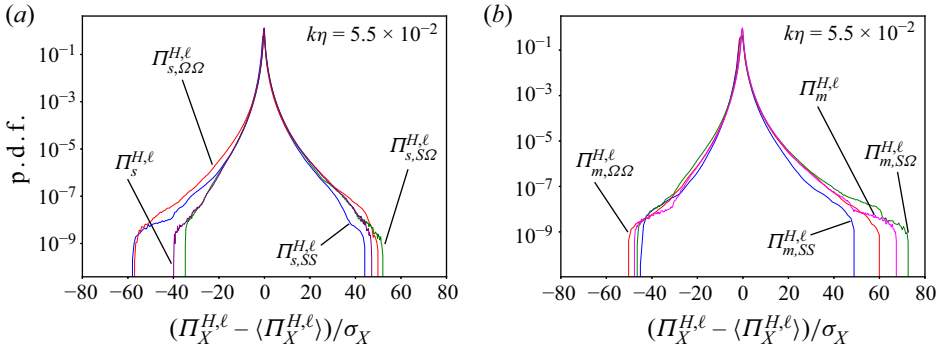

Figure 3. Standardised p.d.f.s of helicity subfluxes $\Pi^{H,\ell}_X$, where X refers to the subflux identifier, for (*a*) single-scale and (*b*) multi-scale contributions; σ_X denotes the standard deviation of each respective term. Values of σ_X are provided in table 2.

	$\Pi^{H,\ell}_s$	$\Pi^{H,\ell}_{s,SS}$	$\Pi^{H,\ell}_{s,S\Omega}$	$\Pi^{H,\ell}_{s,\Omega\Omega}$	$\Pi^{H,\ell}_m$	$\Pi^{H,\ell}_{m,SS}$	$\Pi^{H,\ell}_{m,S\Omega}$	$\Pi^{H,\ell}_{m,\Omega\Omega}$
σ^2_X	1763	159	1200	248	563	53	283	72
$\dfrac{\langle(\Pi^{H,\ell}_X)^3\rangle}{\sigma^3_X}$	0.57	−0.34	0.42	−0.48	0.75	−1.62	0.39	−0.49
$\dfrac{\langle(\Pi^{H,\ell}_X)^4\rangle}{\sigma^4_X}$	24.0	22.6	23.1	34.2	27.6	19.58	34.6	27.9

Table 2. Values of variance, skewness and flatness for the subflux p.d.f.s at $k\eta = 0.055$ shown in figure 3.

magnitude of helicity backscatter. Figure 3 presents standardised probability density functions (p.d.f.s) of all helicity subfluxes at $k\eta = 5.5 \times 10^{-2}$, which is approximately in the inertial range. These p.d.f.s have wide tails, and are strongly non-Gaussian. Single- and multi-scale terms all have strong fluctuations between 60 and 75 standard deviations. Interestingly, the subflux term $\Pi^{H,\ell}_{s,\Omega\Omega}$, which necessarily vanishes in mean (see (2.18)), has the strongest fluctuations (i.e. is the most intermittent).

Values of the variance, skewness and flatness for each of the p.d.f.s shown in figure 3 are provided in table 2. All p.d.f.s are more symmetric than for the kinetic energy fluxes (Johnson 2021) (not shown) with generally low skewness values. The p.d.f.s of $\Pi^{H,\ell}_s$, $\Pi^{H,\ell}_{s,S\Omega}$, $\Pi^{H,\ell}_m$ and $\Pi^{H,\ell}_{m,S\Omega}$ are slightly positively skewed while the p.d.f.s of $\Pi^{H,\ell}_{s,SS}$, $\Pi^{H,\ell}_{m,SS}$ and $\Pi^{H,\ell}_{m,\Omega\Omega}$ are slighly negatively skewed. The symmetry is more pronounced in the single-scale rather than the multi-scale terms, as can be seen by comparison of the left and right panels of figure 3, and by comparison of the skewness values reported in table 2. As all averaged fluxes (except $\langle\Pi^{H,\ell}_{s,\Omega\Omega}\rangle$ which is zero) transfer positive helicity from large to small scales, symmetry in the p.d.f.s indicates strong backscatter of positive helicity, or forward scatter of negative helicity. The p.d.f.s become even broader with decreasing filter scale (not shown). A comparison between the p.d.f.s of $\Pi^{H,\ell}$ and the alternative description based on SGS stresses related to vortex stretching, $\tilde{\Pi}^{H,\ell}$, has been carried out by Yan *et al.* (2020), indicating more intense backscatter in the latter compared with

the former. Adding or removing a total gradient can strongly reduce the negative tail of the SGS energy transfer (Vela-Martín 2022), and the same may apply to the helicity flux.

5. Conclusions

We have derived an exact decomposition of the helicity flux across scales in terms of interactions between vorticity gradients and velocity gradients, and in terms of their scale locality. Decomposing all gradient tensors into symmetric and antisymmetric parts allows for a discussion and quantification of different physical mechanisms that constitute the helicity cascade. Simulation results indicate that all subfluxes transfer helicity from large to small scales, albeit with strong backscatter. In the inertial range, approximately 50 % of the total mean helicity flux is due to the action of two scale-local processes: (i) vortex flattening and (ii) vortex twisting. We have also shown that these two effects are related in mean through a newly derived exact (Betchov-type) relation, which implies that the contribution of the former is exactly three times larger than that of the latter. Multi-scale effects account for the remaining 50 %, with approximate equipartition between multi-scale versions of the two aforementioned effects and multi-scale vortex entangling. Thus, it seems likely that, in LES contexts, accurate modelling of the helicity cascade should not neglect the multi-scale contributions. Although our numerical quantification of the fluxes is obtained using data from a single simulation with an inertial range of limited length, we conjecture that the results obtained are robust in the sense that we expect them to hold for flows with larger Reynolds numbers. Increasing resolution and Reynolds number is certainly a key step to understand whether single-scale and multi-scale contributions are Reynolds-number independent in the asymptotic limit. We may address this point quantitatively in the future. A brief discussion of Reynolds-number effects and results at lower Reynolds number is provided in the Appendix. Similar flux decompositions can be derived for magnetohydrodynamics. We will report results of these investigations elsewhere in due course.

Funding. Computational resources were provided through Scottish Academic Access on Cirrus (www.cirrus.ac.uk), and the UK Turbulence Consortium on ARCHER2 (www.archer2.ac.uk). This work received funding from the European Research Council (ERC) under the European Union's Horizon 2020 research and innovation programme (grant agreement no. 882340) and from the Priority Programme SPP 1881 'Turbulent Superstructures' of the Deutsche Forschungsgemeinschaft (DFG, Li3694/1).

Declaration of interests. The authors report no conflict of interest.

Author ORCIDs.
Damiano Capocci https://orcid.org/0000-0002-0497-0165;
Perry L. Johnson https://orcid.org/0000-0002-7929-9396;
Sean Oughton https://orcid.org/0000-0002-2814-7288;
Luca Biferale https://orcid.org/0000-0001-8767-9092;
Moritz Linkmann https://orcid.org/0000-0002-3394-1443.

Appendix. Reynolds-number effects

In order to discuss Reynolds-number effects in connection with the formation of plateaux for the subfluxes, we carried out an additional simulation at lower Reynolds number, $Re_\lambda = 240$, on 512 collocation points in each spatial direction and a resolution of $k_{max}\eta = 1.25$. Data was averaged over 40 equispaced snapshots separated in time by 0.6 large-eddy turnover times. Figure 4 presents the helicity subfluxes. In comparison with the data shown in the figure and the higher-Re_λ data presented in figure 2, we note that plateaux are less

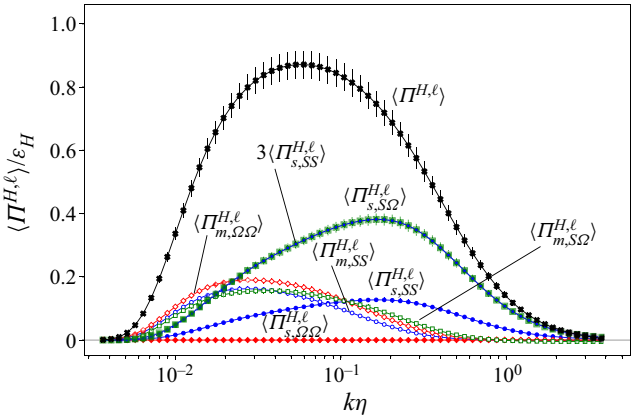

Figure 4. Decomposed helicity fluxes normalised with the mean helicity dissipation rate ε_H for $Re_\lambda = 240$. Filled markers correspond to single-scale contributions while empty symbols are related to multi-scale contributions. The error bars indicate one standard error.

extended for the multi-scale terms in the lower-Re_λ data, and that no plateau-formation is visible in the single-scale terms. In contrast, for the higher-Re_λ data, the single-scale terms are less scale-dependent in the (approximate) inertial range. It is thus plausible that with increasing Reynolds number plateaux form, and indeed become more extended, for all non-vanishing mean subfluxes.

References

Alexakis, A. 2017 Helically decomposed turbulence. *J. Fluid Mech.* **812**, 752–770.

Alexakis, A. & Biferale, L. 2018 Cascades and transitions in turbulent flows. *Phys. Rep.* **767–769**, 1–101.

Baerenzung, J., Politano, H., Ponty, Y. & Pouquet, A. 2008 Spectral modeling of turbulent flows and the role of helicity. *Phys. Rev.* E **77**, 046303.

Betchov, R. 1956 An inequality concerning the production of vorticity in isotropic turbulence. *J. Fluid Mech.* **1**, 497–504.

Biferale, L., Musacchio, S. & Toschi, F. 2012 Inverse energy cascade in three-dimensional isotropic turbulence. *Phys. Rev. Lett.* **108**, 164501.

Biferale, L., Musacchio, S. & Toschi, F. 2013 Split energy-helicity cascades in three dimensional homogeneous and isotropic turbulence. *J. Fluid Mech.* **730**, 309–327.

Brandenburg, A. 2001 The inverse cascade and nonlinear alpha-effect in simulations of isotropic helical magnetohydrodynamic turbulence. *Astrophys. J.* **550**, 824–840.

Brandenburg, A. & Subramanian, K. 2005 Astrophysical magnetic fields and nonlinear dynamo theory. *Phys. Rep.* **417**, 1–209.

Brissaud, A., Frisch, U., Léorat, J., Lesieur, M. & Mazure, A. 1973 Helicity cascades in fully developed isotropic turbulence. *Phys. Fluids* **16**, 1366–1367.

Carbone, M. & Wilczek, M. 2022 Only two Betchov homogeneity constraints exist for isotropic turbulence. *J. Fluid Mech.* **948**, R2.

Chen, Q., Chen, S. & Eyink, G.L. 2003*a* The joint cascade of energy and helicity in three-dimensional turbulence. *Phys. Fluids* **15**, 361–374.

Chen, Q., Chen, S., Eyink, G.L. & Holm, D.D. 2003*b* Intermittency in the joint cascade of energy and helicity. *Phys. Rev. Lett.* **90**, 214503.

Constantin, P. & Majda, A. 1988 The Beltrami spectrum for incompressible flows. *Commun. Math. Phys.* **115**, 435–456.

Deusebio, E. & Lindborg, E. 2014 Helicity in the Ekman boundary layer. *J. Fluid Mech.* **755**, 654–671.

Eyink, G.L. 2005 Locality of turbulent cascades. *Physica* D **207**, 91–116.

Eyink, G.L. 2006 Multi-scale gradient expansion of the turbulent stress tensor. *J. Fluid Mech.* **549**, 159–190.

Germano, M. 1992 Turbulence — the filtering approach. *J. Fluid Mech.* **238**, 325–336.

GLEDZER, E.B. & CHKHETIANI, O.G. 2015 Inverse energy cascade in developed turbulence at the breaking of the symmetry of helical modes. *J. Expl Theor. Phys. Lett.* **102**, 465–472.

HERRING, J.R. 1974 Approach of axisymmetric turbulence to isotropy. *Phys. Fluids* **17**, 859–872.

INAGAKI, K., YOKOI, N. & HAMBA, F. 2017 Mechanism of mean flow generation in rotating turbulence through inhomogeneous helicity. *Phys. Rev. Fluids* **2**, 114605.

JOHNSON, P.L. 2020 Energy transfer from large to small scales in turbulence by multiscale nonlinear strain and vorticity interactions. *Phys. Rev. Lett.* **124**, 104501.

JOHNSON, P.L. 2021 On the role of vorticity stretching and strain self-amplification in the turbulence energy cascade. *J. Fluid Mech.* **922**, A3.

KESSAR, M., PLUNIAN, F., STEPANOV, R. & BALARAC, G. 2015 Non-Kolmogorov cascade of helicity-driven turbulence. *Phys. Rev.* E **92**, 031004(R).

KRAICHNAN, R. 1973 Helical turbulence and absolute equilibrium. *J. Fluid Mech.* **59**, 745–752.

LI, Y., MENEVEAU, C., CHEN, S. & EYINK, G.L. 2006 Subgrid-scale modeling of helicity and energy dissipation in helical turbulence. *Phys. Rev.* E **74**, 026310.

LILLY, D.K. 1986 The structure, energetics, and propagation of rotating convective storms. Part II: helicity and storm stabilization. *J. Atmos. Sci.* **43**, 126–140.

LINKMANN, M. 2018 Effects of helicity on dissipation in homogeneous box turbulence. *J. Fluid Mech.* **856**, 79–102.

LINKMANN, M.F., BERERA, A., MCKAY, M.E. & JÄGER, J. 2016 Helical mode interactions and spectral energy transfer in magnetohydrodynamic turbulence. *J. Fluid Mech.* **791**, 61–96.

LINKMANN, M.F., SAHOO, G., MCKAY, M.E., BERERA, A. & BIFERALE, L. 2017 Effects of magnetic and kinetic helicities on the growth of magnetic fields in laminar and turbulent flows by helical Fourier decomposition. *Astrophys. J.* **836**, 26.

MILANESE, L.M., LOUREIRO, N.F. & BOLDYREV, S. 2021 Dynamic phase alignment in Navier–Stokes turbulence. *Phys. Rev. Lett.* **127**, 274501.

MININNI, P.D. & POUQUET, A.G. 2010*a* Rotating helical turbulence. I. Global evolution and spectral behavior. *Phys. Fluids* **22**, 035105.

MININNI, P.D. & POUQUET, A.G. 2010*b* Rotating helical turbulence. II. Intermittency, scale invariance, and structures. *Phys. Fluids* **22**, 035106.

MOFFATT, H.K. 1969 The degree of knottedness of tangled vortex lines. *J. Fluid Mech.* **35**, 117–129.

MOFFATT, H.K. 2014 Helicity and singular structures in fluid dynamics. *Proc. Natl Acad. Sci.* **111** (10), 3663–3670.

SAHOO, G., ALEXAKIS, A. & BIFERALE, L. 2017 Discontinuous transition from direct to inverse cascade in three-dimensional turbulence. *Phys. Rev. Lett.* **118**, 164501.

SAHOO, G., BONACCORSO, F. & BIFERALE, L. 2015 Role of helicity for large- and small-scale turbulent fluctuations. *Phys. Rev.* E **92**, 051002.

SCHEELER, M.W., VAN REES, W.M., KEDIA, H., KLECKNER, D. & IRVINE, W.T.M. 2017 Complete measurement of helicity and its dynamics in vortex tubes. *Science* **357**, 487–491.

STEENBECK, M., KRAUSE, F. & RÄDLER, K.-H. 1966 Berechnung der mittleren Lorentz–Feldstärke v x B für ein elektrisch leitendes Medium in turbulenter, durch Coriolis–Kräfte beeinflußter Bewegung. *Z. Naturforsch.* A **21**, 369–376.

STEPANOV, R., GOLBRAIKH, E., FRICK, P. & SHESTAKOV, A. 2015 Hindered energy cascade in highly helical isotropic turbulence. *Phys. Rev. Lett.* **115**, 234501.

TOBIAS, S.M., CATTANEO, F. & BOLDYREV, S. 2013 MHD dynamos and turbulence. In *Ten Chapters in Turbulence* (ed. P.A. Davidson, Y. Kaneda, & K.R. Sreenivasan). Cambridge University Press.

VELA-MARTÍN, A. 2022 Subgrid-scale models of isotropic turbulence need not produce energy backscatter. *J. Fluid Mech.* **937**, A14.

WALEFFE, F. 1992 The nature of triad interactions in homogeneous turbulence. *Phys. Fluids* A **4**, 350–363.

YAN, Z., LI, X., YU, C., WANG, J. & CHEN, S. 2020 Dual channels of helicity cascade in turbulent flows. *J. Fluid Mech.* **894**, R2.

YOKOI, N. & YOSHIZAWA, A. 1993 Statistical analysis of the effects of helicity in inhomogeneous turbulence. *Phys. Fluids* A **5**, 464–477.

YU, C, HU, R., YAN, Z. & LI, X. 2022 Helicity distributions and transfer in turbulent channel flows with streamwise rotation. *J. Fluid Mech.* **940**, A18.